Jing *et al. Biochar* (2026) 8:38
https://doi.org/10.1007/s42773-025-00555-y

Biochar

ORIGINAL RESEARCH Open Access

Dynamic contact angle as a new metric for the water repellency evaluation of biochar-amended soil

Wei Jing[1,2,3,4], Mingjie Su[1,5,6], Kai Yang[1,2,4], Qilin Kang[1,5,6], Yaoming Li[1,5,6], Wei Li[1,2,4], Kun Zhang[2,4*] and Jiefei Mao[1,5,6*]

Abstract

Biochar hydrophobicity is crucial for understanding its interaction with environmental substances (e.g., soil, water, pollutants). Contact angle (CA) and water droplet penetration time (WDPT) are commonly used methods for assessing biochar hydrophobicity. However, occasional inconsistencies between CA and WDPT measurements introduce uncertainties, emphasizing the need for more accurate evaluation. This study addressed these temporal inconsistencies by proposing a new method using the dynamic contact angle (DCA) to evaluate the hydrophobicity of 17 standard materials and 18 types of biochars. The DCA method, which considers droplet diffusion recorded CA changes over 90 s and compared the significance ($p < 0.05$) between initial CA (CA_0) and CA after 90 s (CA_90). Based on this, a new classification of hydrophobicity was established, encompassing super-hydrophobic, strongly hydrophobic, 'pseudo'-hydrophobic and hydrophilic categories. 'Pseudo'-hydrophobic materials exhibited a significant decrease in CA within 90 s, where the CA transitioned from hydrophobic (CA > 90°) to hydrophilic (CA < 90°) within this period, revealing their hydrophilic nature. The combination of CA_0 and the rate of CA change over time ($|k|$) was considered as a new criterion for hydrophobicity evaluation. Through a 90-day incubation experiment of biochar and soil, most biochars significantly increased the water repellency of the biochar-amended soil, as evidenced by increases in both CA_0 and CA_90. Our DCA method, along with the definition 'pseudo'-hydrophobicity, resolves contradictions between CA and WDPT measurements for both soil and biochar, enhancing the accuracy of hydrophobicity assessments.

Highlights

- A droplet diffusion-based dynamic contact angle (DCA) method was newly proposed to evaluate the hydrophobicity of biochar.
- A new category 'pseudo' hydrophobicity was introduced in the classification of hydrophobicity.
- The DCA method addressed inconsistencies between contact angle and water drop penetration time measurements.

Keywords 'Pseudo' hydrophobicity, Contact angle, Soil water repellency, Water diffusion, Biochar amendment

*Correspondence:
Kun Zhang
kzhang@xju.edu.cn
Jiefei Mao
mjf@ms.xjb.ac.cn
Full list of author information is available at the end of the article

Springer

Graphical Abstract

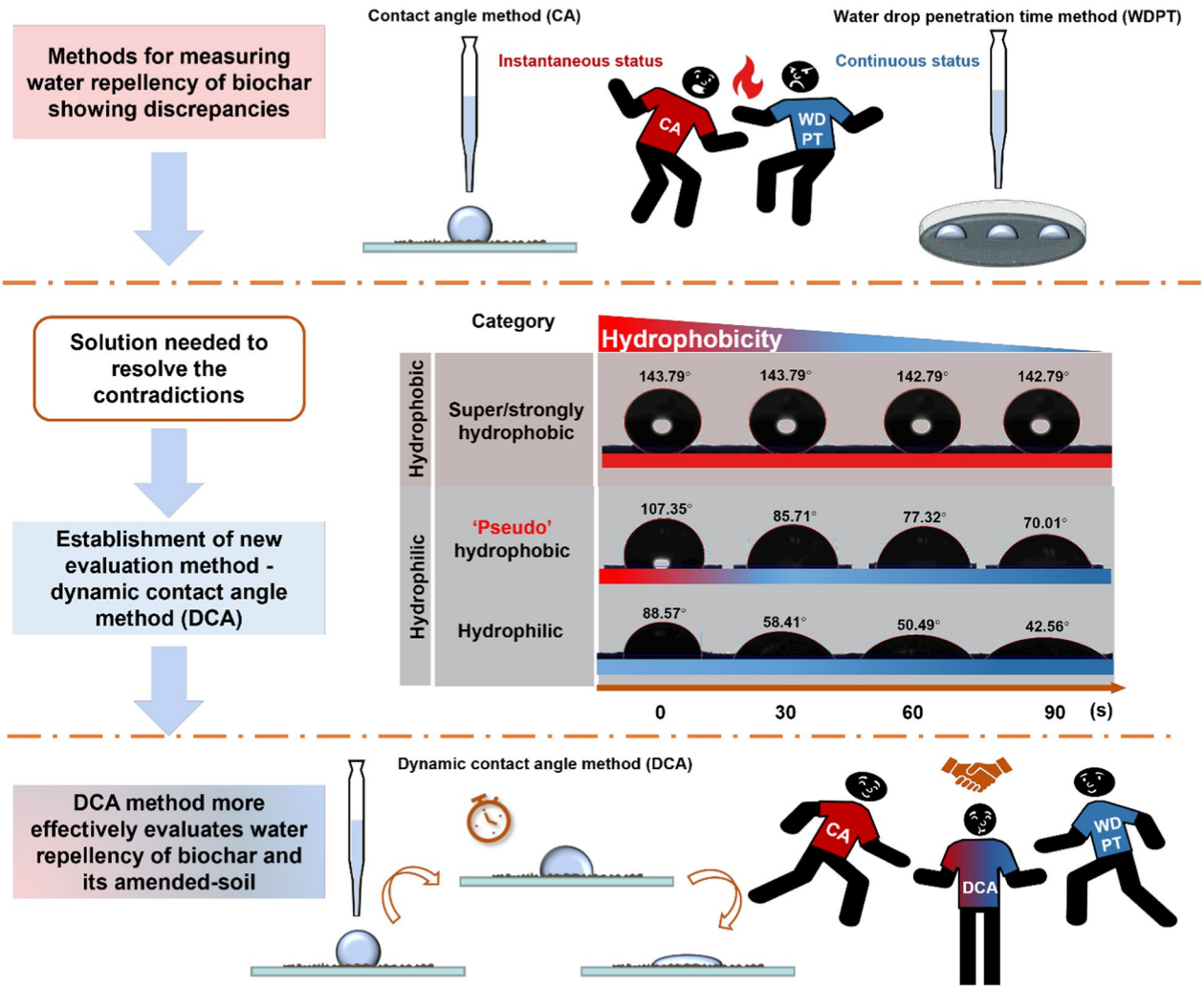

1 Introduction

Drylands constitute approximately 41% of the Earth's land area (Schlaepfer et al. 2017). These regions are characterized by unpredictable precipitation patterns, exhibiting substantial spatial and temporal variations (Ding et al. 2021), alongside high evaporation rates. Such conditions render these areas particularly vulnerable to drought stress. Moreover, the soils in these areas have an inadequate structure and low water retention capacity, adversely affecting plant growth (Alghamdi et al. 2020). Consequently, enhancing soil water retention in arid and semi-arid regions is of great importance. The current techniques for enhancing soil water include the use of straw mulching (Wang et al. 2018), the incorporation of soil with high water retention capacity, and the addition of water-retaining agents. Among these, biochar has emerged as a widely used water-retaining agent, with the potential to significantly improve soil structure and promote plant growth (Haddad et al. 2022; Zhang et al. 2023; Xu et al. 2024).

Biochar is typically defined as a carbon-rich, solid organic material produced through the pyrolysis of biomass under anaerobic or oxygen-limited conditions (Roberts et al. 2010; Muema et al. 2024). As a common soil conditioner, biochar positively affects soil physicochemical properties by reducing soil bulk density, increasing soil porosity (Baiamonte et al. 2019; Seitz et al. 2020) and air permeability (Villagra-Mendoza and Horn 2018), and optimizing soil structure (Wang et al. 2019; Yang and Lu 2021). Its large specific surface area and abundant pore

volume contribute to a significant increase in soil water holding capacity (Santos et al. 2022). Additionally, the hydrophilic functional groups present in biochar, such as carboxyl and hydroxyl, have been shown to directly enhance soil water retention (Zhang et al. 2024).

Hydrophobicity, also known as water repellency (WR), refers to the phenomenon wherein water encounters difficulty or even impossibility in wetting a solid surface (DeBano 2000). Soil water repellency (SWR) reduces the rate of soil infiltration (Li et al. 2018; Paz et al. 2024), subsequently leading to a decline in soil water retention (Albalasmeh and Mohawesh 2023). The addition of biochar into soil can alter SWR (Acharya et al. 2024), which may either increase or decrease the water holding capacity of soil depending on the physicochemical properties of the biochar (Adhikari et al. 2022). For instance, Fu et al. (2019) reported that the hydrophobicity of biochar inhibits its positive impact on soil water retention. In contrast, Mao et al. (2019) found that hydrophobic biochar increased the SWR, and the increment became more pronounced with the larger biochar addition. They observed that hydrophobic biochar could improve the water holding capacity of non-water-repellent soil with low organic carbon content. These findings underscore the necessity for further investigation to elucidate the relationship between biochar hydrophobicity and soil water retention. Moreover, leveraging biochar to modulate SWR and thereby improve soil water retention represents a promising strategy for arid and semi-arid regions.

Various methodologies have been developed to assess water repellency, among which the contact angle (CA) method (Huhtamäki et al. 2018) and the water droplet penetration time (WDPT) method (Doerr et al. 1998) are particularly noteworthy. Each of these techniques offers specific advantages and limitations in practical additions. The CA method, renowned for its precision, is particularly well-suited for meticulous measurements in controlled laboratory settings. However, it primarily measures the initial CA of water droplets, which delineates the instantaneous water repellency of the solid surface. A number of studies have observed a decrease in CA of water droplets on solid materials over time (Leelamanie and Karube 2009; Papierowska et al. 2018), indicating that the initial CA alone may not be adequate to represent the sustained hydrophobicity of such materials. Conversely, the WDPT method is straightforward and convenient for field measurements. However, surface tension-induced adhesion between solids and droplets causes measurement inaccuracies (Usevičiūtė and Baltrėnaitė 2020). In short, the initial CA reflects instantaneous hydrophobicity, while the penetration time provides insight into persistent hydrophobic characteristics. Given the complex nature of biochar, characterized by diverse geometries, both widely used methods exhibit limitations to varying degrees in accurately determining its hydrophobicity. Additionally, due to the multifaceted interactions at both physical and chemical levels, these methodologies may introduce measurement errors and result in inconsistencies. In general, soil is considered water repellent if its CA > 90° or WDPT > 5 s, whereas non-water-repellent soil typically shows an initial CA < 90° and its WDPT < 5 s, respectively (Buczko and Bens 2006). However, some studies found that the mixture of biochar and soil had an initial CA > 90° (indicating water repellency), while the corresponding WDPT was < 5 s (indicating non-water-repellency) (Liu et al. 2022). The discrepancies between CA and WDPT measurements are primarily attributed to structural differences between tested materials and the rigid matrix of mineral soils, where the widely applied WDPT method exhibits significant limitations (Liu et al. 2022). As demonstrated by Müller (2016), WDPT failed to detect subcritical SWR—a phenomenon where soils exhibit apparent water absorption while remaining influenced by water-repellent surface distributions (Hallett et al. 2001). Additionally, variations in measurement conditions and methods contribute to inconsistent water repellency assessments of soils (Aranda et al. 2016; Cervera-Mata et al. 2021; Hewelke et al. 2023). However, it is worth noting that this contradictory phenomenon may also be ascribed to the fact that the initial CA measures the instantaneous hydrophobicity of the material surface, while the WDPT evaluates hydrophobicity over a longer time frame. The temporal discrepancy between the two methods necessitates the identification of an appropriate approach to reconcile this paradox. Further analysis suggests that the initial CA does not account for diffusion behavior, while the WDPT incorporates this factor. Consequently, the emerging paradox can be explained by the diffusion of water droplets. Due to these inherent limitations, the initial CA is not the optimal criterion for determining the hydrophobicity of biochar. Therefore, this study emphasizes the importance of combining both methods and evaluating hydrophobicity considering both contact angle and diffusion processes.

Thus, the diffusion of water droplets on solid surface should be taken into account to determine water repellency. To investigate the influence of water diffusion on CA measurement of biochar hydrophobicity, this study employed dynamic CA to evaluate biochar hydrophobicity. Given the heterogeneity of biochar (Zhang et al. 2019), the materials with simple structure and homogeneous compositions were initially selected to establish a new hydrophobicity assessment method. Meanwhile, to ensure the representativeness of the hydrophobicity evaluation, the CA measurements should cover the range of

0°–180°. Considering these factors, 17 standard materials, including metals and their oxides, microplastics, and graphite, were selected to observe the CA changes until they became constant. The dynamic CA of all materials was compared with their initial CA and WDPT, leading to an updated category of surface hydrophobicity. A new evaluation method for surface hydrophobicity was developed based on dynamic CA. Using the new approach, the hydrophobicity of 18 types of biochar was evaluated. Furthermore, the changes in SWR under different addition conditions over a period of 90 days were investigated for 18 types of biochars using the newly established method. This study can accurately assess the hydrophobicity of complex and heterogeneous substances, for instance, biochar and soil. It offers crucial insights for biochar addition in environmental contexts, soil amendments, and functional material design.

2 Materials and methods

2.1 Standard material selection

Considering the variations in biomass, pyrolysis temperatures, residence times, and other factors during biochar production, the resulting biochars exhibit complex surface morphologies, diverse shapes, varying particle sizes, and high heterogeneity. Establishing a direct evaluation method for such a wide range of characteristics is highly challenging and may not adequately cover the contact angle range of 0° to 180°. Therefore, this study initiated with simple pure substances, selecting 17 standard materials to construct an evaluation framework for assessing the hydrophobic and diffusion behaviors of water on surfaces with different structures. Information on the purity and manufacturer of the standard materials is given in Table S1. Standard materials were named according to the convention 'element/substance name, shape, mesh number'. For instance, the name label of "Fe sheet 100" represented the pure iron sized at 100 mesh with sheet shape. The following abbreviations were used for polymers in this study: polystyrene (PS), polypropylene (PP), polytetrafluoroethylene (PTFE), polyethylene (PE), and nylon (66) (PA (66)).

2.2 Biochar preparation

The biomasses were selected according to the utilization of sustainable resources, encompassing three representative categories of waste materials: agricultural residues (wheat straw (WS) and cotton stalk (CS)), forestry byproducts (poplar wood sawdust (PT), pinewood sawdust (PW), and pine needles (PN)), and household biowaste (tangerine peels (TP)).All the six biomasses, WS, CS, PT, PW, TP, and PN were pulverized and sieved. The sieved biomass was subjected to oxygen-limited pyrolysis using a muffle furnace (KSL-1200X-M, HF-Kejing, China) for 6 h at target temperatures (300, 500, and 700 °C). After cooling to room temperature, the biochar was sieved through a 0.15 mm sieve for use. The biochars with different pyrolysis temperatures were designated as WS300, WS500, WS700, CS300, CS500, CS700, PT300, PT500, PT700, PW300, PW500, PW700, TP300, TP500, TP700, PN300, PN500, PN700, respectively.

2.3 Biochar characterization

The elemental composition (e.g., C, H, N, and S) of the biochar was determined using an elemental analyzer (UNICUBE, Elementar, Germany). The surface functional groups of biochar were analyzed using a Fourier transform infrared (FTIR) spectrometer (Nicolet 6700, Thermo Scientific, USA). The FTIR spectral range was recorded from 400 to 4000 cm^{-1} with a resolution of 1 cm^{-1}. The content of O was calculated using the difference method. Elemental compositions and atomic ratios were corrected for ash. The ash content was determined by pyrolyzing biochar at 800 ℃ for 4 h. The surface area and pore volume of biochar were measured by an automatic physical adsorption instrument (ASAP 2460, Micromeritics, USA) using N_2 as a measuring gas. The pH was determined by placing biochar in a container with ultrapure water at a ratio of 1:20 (w/w), and measuring shaking and settling, where the pH of biochar was measured by a pH meter (SevenExcellence, Mettler Toledo, Switzerland) (Inyang et al. 2012; Xue et al. 2012). Relevant data are shown in Table S2.

2.4 Determination of contact angle and WDPT

The material was evenly spread on the double-sided adhesive tape (65×15 mm) on the slide. For each material (standard material, biochar, biochar-added soil), three slides were used and three droplets were placed at equal intervals on each slide, resulting in a total of 9 droplets for CA measurement. A water droplet of 10 μL was placed on the material using the electric injection system of contact angle meter (SDC-200ST, SINDIN, China). According to our preliminary CA measurement, for the majority of standard materials, the CA of each droplet did not fluctuate after 80 s, while for others it stabilized after 90 s (Fig. S2). Thus, to minimize the impact of evaporation on the CA during the test, the CA was recorded from 0 to 90 s with an interval of 10 s. The CA measured at 0 s and 90 s were defined as initial CA (CA_0) and CA_90, respectively. Generally, surfaces with contact angles greater than 90° are considered hydrophobic. Conversely, surfaces with contact angles between 0° and 90° are considered hydrophilic (Doerr et al. 2000). Surfaces with contact angles near or above 150° are

classified as super hydrophobic (Zhang et al. 2008). Three parallel slides were used for each sample, and three drops were placed on each slide. The average CA of the 9 droplets was calculated, ensuring the reliability and reproducibility of the obtained results.

The WDPT was determined by placing the standard materials and biochar uniformly in an aluminum box, placing a water droplet (36 μL) on the material surface, and recording the complete penetration time of the droplets. At least 9 water droplets were used for each sample and the penetration time was observed separately. The standard materials and biochar were categorized into five groups based on the penetration time: WDPT < 5 s (hydrophilic); 5 s ≤ WDPT ≤ 60 s (slightly hydrophobic); 60 s < WDPT ≤ 600 s (strongly hydrophobic); 600 s < WDPT ≤ 3600 s (severely hydrophobic); and WDPT > 3600 s (extremely hydrophobic) (Bisdom et al. 1993). Both CA and WDPT methods were performed at 22 ± 2 ℃ and relative humidity (RH) of 35 ± 2%.

2.5 Soil sampling and soil-biochar incubation

The soil utilized in this study was collected from the topsoil layer (0–20 cm depth) of farmland located within the Xinjiang Fukang Desert Ecosystem Observation and Research Station of the Chinese Academy of Sciences (44°17' N, 87°56' E). The soil was air-dried, ground, and passed through a 2 mm sieve, and subsequently stored in bags for further analysis. The soil pH was measured using a pH meter at a soil-to-water ratio of 1:2.5 (w/w). A laser particle size analyzer (MasterSizer 2000, Malvern, UK) was utilized to determine the particle size distribution of the soil. The soil bulk density and field capacity were determined using the core cutter method. The basic physical and chemical properties of the soil are presented in Table S3.

All types of biochar were evenly mixed with soil at addition rates of 1% and 5%, and the mixtures were placed in aluminum foil boxes with covers. The soil without any biochar addition was set as the control group. Each treatment was prepared in three replicates. To mimic the condition of agricultural soil in arid and semi-arid regions, the soil moisture for the soil-biochar incubation was set at 55% of the field capacity. To maintain the soil moisture of the incubated soil, distilled water was added to the incubated soil once every 3–5 days to counteract water loss from evaporation. The soil-biochar incubation was conducted for 3 months, and the soil-biochar mixture was sampled on the day 0 and day 90 of the duration.

2.6 Measurement of relative porosity, 'shortest' flow path, and surface roughness

To understand the correlation between the CA of solid surface with its physical properties, surface roughness, relative porosity, and the shortest water flow paths of the standard materials as the typical surficial properties were analyzed. Relative porosity refers to the area occupied by the sample in a certain area. The shortest water flow paths are the shortest distances for water to spread from the observation center to the observation edge. A 3D feature scanner (VK-X1000, Keyence, Japan) was used to scan the surface roughness of the material. Specifically, the material was evenly spread on a glass slide and observed under a 5 × magnifying lens. The scanning range was set at 1 × 1 mm^2, and the surface profile was scanned using a laser. Each material was scanned 9 times. The analysis was conducted using the automatic roughness analysis application (AI-Analyzer) to obtain the Ra value. The slide with the sample was placed under a stereo microscope (XTL-165, Phenix, China), viewed at 20 × magnification, and an image of the material surface was captured using the accompanying software. The relative porosity and 'shortest' flow path were determined using Image J software. Relative porosity was calculated by the ratio of the sum of the areas occupied by the samples in the image to the total area of the image. The 'shortest' flow channel was determined by calculating the captured image for the 'shortest' flow channel in four directions (0°, 90°, 180°, and 270°), of which the details are found in Fig. S3.

2.7 Data analysis

The statistical analysis of the data was conducted using SPSS software (IBM SPSS Statistics 20). The Tukey test (for homogeneous variance data) or the Dunnett T3 test (for heterogeneous variance data) was used to explain the significant differences between CA_0 and CA_90. The correlation between ΔCA_90 of the biochar-added soil and the properties of the biochar was analyzed through Pearson correlation analysis (for normally distributed data). The correlations between the surface structure and chemical properties as well as water repellency (CA_0, CA_90) of biochar were obtained through Pearson correlation and Spearman correlation (for non-normally distributed data).The differences between CA_0 for standard materials, biochar, and soil under different biochar addition rates and incubation periods were compared by Duncan's Multiple Range test within the analysis of variance (ANOVA). A linear fit was applied to the CA change over 90 s for the biochar and standard material to obtain the corresponding linear slope $|k|$. The relative contributions of relative porosity, the 'shortest' flow path, and surface roughness to the rate of change of contact angle were analyzed using a random forest model. All image information processing was performed using Image J software.

3 Results and discussion

3.1 Hydrophobicity evaluation of standard materials

When comparing the CA_0 of the 17 standard materials (Table 1), distinct differences were observed among the metals, metal oxides, and polymers. The largest CA_0 was 147.50°, recorded for Cu dendriform 200, while the lowest CA_0 (26.67°) was observed for Al_2O_3 100–200. It should be noted that due to its strongly hydrophilic nature, SiO_2 100 does not allow for accurate measurements of contact angles and penetration time, and thus it is not be discussed further in this study. Notably, the CA_0 for Fe sheet 100 (92.93°) was significantly lower that for and Fe sheet 200 (105.69°), although, there was no significant difference between the CA_0s of Fe spheres 100 and Fe spheres 200. Additionally, the Fe in sheet form exhibited a significantly larger CA_0 compared to Fe in spherical form. Similar findings were also reported in Saha et al. (2020), who found that granular biochar is more hydrophobic than powdered biochar. It suggested that both size and shape could influence the CA_0 of materials, indicating that the regularity of surface morphology may be a factor affecting the CA_0. With the same shape and size, the CA_0 of Fe sphere 200 was significantly lower than that of Cu sphere 200, highlighting the effect of chemical composition on surface hydrophobicity of materials.

The mean WDPT and corresponding hydrophobic level of the 17 standard materials are presented in Table 1. The extremely hydrophobic materials were all the forms of Cu and microplastics, while all the forms of Fe and Al_2O_3 100–200 were hydrophilic, with the WDPT less than 5 s. Interestingly, despite the hydrophilic surface observed in Fe sheets based on WDPT, these materials were classified as hydrophobic based on their CA_0 (> 90°). This result aligns with previous studies (Usevičiūtė and Baltrėnaitė 2020), such as the study by Liu et al. (2022) which classified the biochar surface as hydrophilic based on WDPT (< 5 s), even though their CA_0 ranged between 105 and 119°, indicating hydrophobicity. This discrepancy arises as CA_0 represents the instantaneous hydrophobicity upon droplet contact with solid surface, while WDPT reflects the persistence of hydrophobicity over time. The lack of temporal alignment between CA and WDPT measurements underscores the need to consider the dynamic change in CA over time as a more comprehensive measure of hydrophobicity.

3.2 Dynamic contact angle (DCA) of standard materials

To address the temporal inconsistency between CA and WDPT methods, this study measured the CA_0 and conducted sequential CA measurements at 10 s intervals for a duration of 90 s. As seen in Fig. S4, the CA_90 of those standard materials did not significantly differ from their CA_0. However, for Fe sheet 100, Fe sheet 200, PA (66) 100, kaolin and $CaSiO_3$ 200, the CA decreased with time (Fig. 1, Table S4). Specifically, compared to CA_0, the CA_90 of all five materials significantly decreased ($p < 0.05$). This reduction in CA may be due to the occupation of surface nanopores by water vapor upon contact, which facilitates diffusion (Gray et al. 2014). For these materials, using CA_0 for hydrophobic evaluation may lead to bias. This effect is most pronounced in $CaSiO_3$ 200, where the CA dropped from 106° to 70° within 90 s, resulting in a transition from hydrophobic to hydrophilic classification.

Broadly speaking, water droplets may remain as discrete droplets in confined areas (static state) or spread and be adsorbed on the surface (dynamic state). This indicates a reduction in the surface tension difference between soil and liquid (Chau et al. 2014). Studies on water-repellent porous media (PM)/soil systems have demonstrated that organic hydrophobic molecules undergo reorientation during water repellency measurements (Wang and Wallach 2020). Temporal changes in CA are recognized as indicators of SWR breakdown (Ogunmokun and Wallach 2024), which indirectly signify progressive weakening of SWR and its transition toward non-water-repellency (Leelamanie and Karube 2009; Chau et al. 2014; Griffo et al. 2024). Consequently, a material whose hydrophobicity continually decreases within 90 s would be considered as 'pseudo'-hydrophobic. As such material cannot maintain hydrophobicity, 'pseudo'-hydrophobicity would be categorized as hydrophilic. This transition from hydrophobicity to hydrophilicity was observed in biochar, where the CA changed over time (Liu et al. 2022). It is confirmed that 'pseudo'-hydrophobicity initially displays temporary hydrophobicity but eventually leads to hydrophilicity. Therefore, the potential effects of 'pseudo'-hydrophobic surfaces on environmental processes merit in-depth investigation in future studies.

Surface morphology (Tian et al. 2022) and the interaction between water and the surface (Monroe et al. 2020; Gray et al. 2014) are related to the variation in hydrophobicity. The relative contribution of the rate of change of contact angle to the relative porosity, the 'shortest' flow path, and the surface roughness is shown in the following equation.

$$F(x) = (0.42\,X_1,\ 0.03X_2,\ 0.55X_3)$$

where: x—change rate of CA (°/s); X_1—relative porosity (%); X_2—the 'shortest' water flow path (mm); X_3—surface roughness (μm).

The Random Forest Model data fitting analysis demonstrated that the order of influence is as follows: surface roughness > relative porosity > the 'shortest' water

Table 1 WDPT and initial contact angle (CA_0) of 17 standard materials

Standard material[a]	WDPT (s)	Hydrophobic level[b]	CA_0 (°)[c]
Fe sheet 100	0.74 ± 0.31	Hydrophilic	92.93 ± 3.37f
Fe sheet 200	0.78 ± 0.11	Hydrophilic	105.69 ± 3.17de
Fe spheres 100	1.40 ± 0.62	Hydrophilic	80.29 ± 4.12g
Fe spheres 200	0.60 ± 0.11	Hydrophilic	77.82 ± 6.02g
Cu spheres 200	> 3600	Extremely hydrophobic	102.32 ± 3.94e
Cu dendriform 200	> 3600	Extremely hydrophobic	147.50 ± 2.31a
Al_2O_3 100–200	0.62 ± 0.15	Hydrophilic	26.67 ± 2.80h
TiO_2 100	389.05 ± 38.59	Strongly hydrophobic	91.98 ± 5.66f
$CaSiO_3$ 200	8.90 ± 2.33	Slightly hydrophobic	106.53 ± 2.02d
PA (66) 100	> 3600	Extremely hydrophobic	106.08 ± 1.92de
PS 100	> 3600	Extremely hydrophobic	126.25 ± 4.17c
PP 100	> 3600	Extremely hydrophobic	139.07 ± 2.97b
PTFE 100	> 3600	Extremely hydrophobic	135.61 ± 4.27b
PE 100	> 3600	Extremely hydrophobic	136.16 ± 3.32b
Graphite 80–120	137.80 ± 39.06	Strongly hydrophobic	136.40 ± 4.28b
Kaolin 100	17.05 ± 3.60	Slightly hydrophobic	108.25 ± 1.85d
SiO_2 100	*	Hydrophilic	*

[a] Standard materials are labelled as 'substance, shape, mesh number', whereas PS, PP, PTFE, PE, and PA (66) are the abbreviations for polystyrene, polypropylene, polytetrafluoroethylene, polyethylene, and nylon (66), respectively

[b] Hydrophobic level here was determined by WDPT method (Bisdom et al. 1993)

[c] Lowercase letters in the column of CA_0 indicate significant differences of CA_0 among the various standard materials ($p \leq 0.05$). *indicates that due to its strongly hydrophilic nature, SiO_2 100 does not allow for accurate measurements of contact angles and penetration times

flow path. This indicates that surface roughness and relative porosity are pivotal factors in the assessment of hydrophobicity through the measurement of dynamic contact angle. While recognizing that other chemical factors may exert a more complex and pronounced influence, this study confined its investigation to the physical-level influencing factors, which is also the direction of further research.

3.3 Establishment of new hydrophobicity evaluation method

Considering the diffusion of water droplets on solid surface and the significant difference between CA_0 and dynamic CA_90, this study proposed a new classification for surface hydrophobicity (Table 2). The hydrophobicity of material surface was set into four categories: (i) Super hydrophobic (CA_0 ≥ 150°, with CA_90 not significantly different from CA_0); (ii) Strongly hydrophobic (CA_0 between 90° and 150°, with CA_90 not significantly different from CA_0); (iii) 'Pseudo'-hydrophobic (CA_0 ≥ 90°, with CA_90 significantly different from CA_0); (iv) Hydrophilic (CA_0 < 90°). In accordance with the new classification, the evaluation method for hydrophobicity can be applied to different types of materials in consideration of their hydrophobicity. The severity of the hydrophobicity of materials followed a descending order: group (i) > group (ii) > group (iii) > group (iv). For materials that are super hydrophobic, strongly hydrophobic, or hydrophilic, their hydrophobicity can be effectively evaluated using CA_90.

The combination of CA_0 and CA_90 provides a qualitative analysis of hydrophobicity across various surfaces. A more detailed quantitative analysis is warranted for materials classified as 'pseudo'-hydrophobic. In these cases, in addition to CA_90, the rate of change in CA ($|k|$) within 90 s is crucial for evaluating hydrophobicity. For instance, in this study, the hydrophobicity of 'pseudo'-hydrophobic materials (Fe sheet 100, Fe sheet 200, PA (66) 100, Kaolin, $CaSiO_3$ 200) was determined by analyzing the rate of change in CA over 90 s. A linear fitting curve was applied to calculate the rate of change in CA for these materials, as shown in Fig. 1.

Comparing the slopes ($|k|$) of the CA curves for 'pseudo'-hydrophobic materials, the hydrophobicity of the material surface is inversely proportional to the slope. Therefore, a larger $|k|$ indicated weaker hydrophobicity, while a smaller $|k|$ suggests stronger hydrophobicity. Based on the combination of CA_90 and $|k|$, the hydrophobicity of the 'pseudo'-hydrophobic standard materials was ranked as follows: PA (66) 100 > Kaolin > Fe sheet 100 > Fe sheet 200 > $CaSiO_3$ 200. In summary, the direct comparison of material hydrophobicity depends on their classification into one of the four groups. Within the same group (i, ii, and iv), CA_90 could be applied to determine the severity of hydrophobicity. For materials categorized in group (iii), the rate of change in CA ($|k|$) is the primary criterion, with CA_90 serving as a second parameter when for $|k|$ values are the same.

3.4 Hydrophobicity of biochars based on CA and WDPT

Through the determination of the basic physical and chemical properties of biochar, the results indicated that the ash content and pH of the biochar exhibited a gradual increase with the elevation of pyrolysis temperature (Table S2). At the same pyrolysis temperature, the ash content of straw-based biochar (CS and WS) was higher

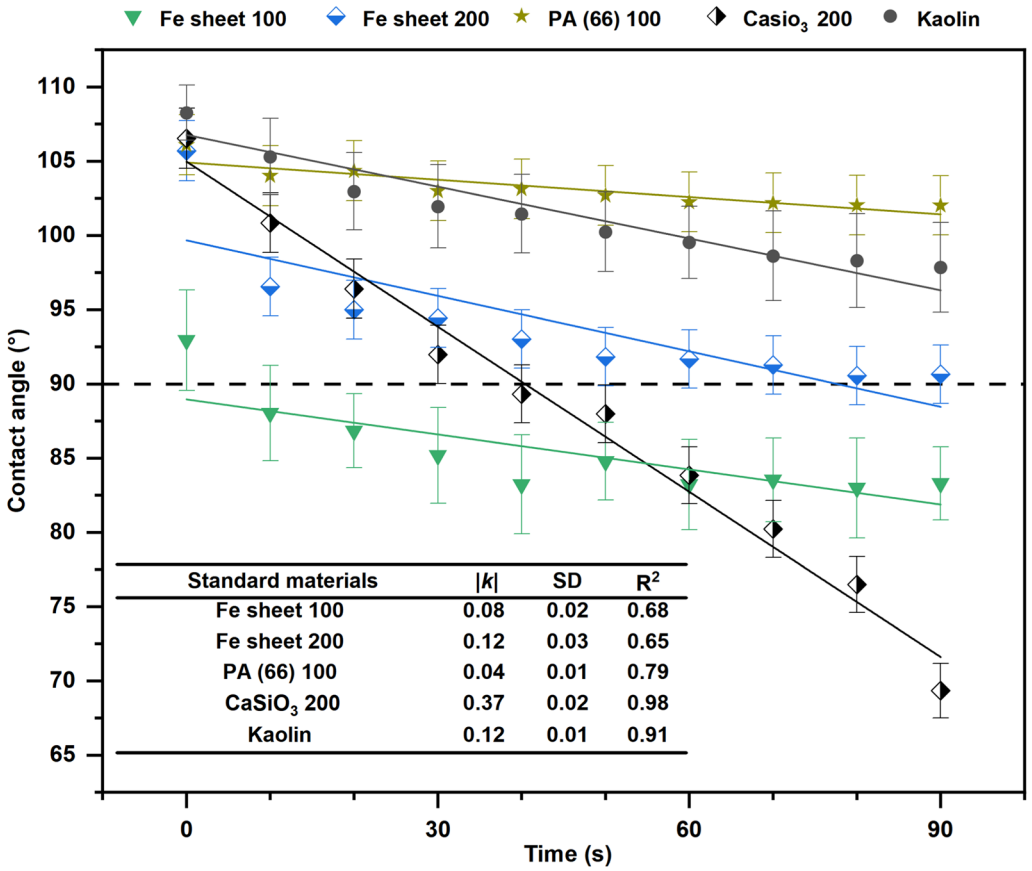

Fig. 1 Linear fitting of contact angle over time for 'pseudo'-hydrophobic standard materials, where |*k*| represents the slope of linear fitting, meaning the rate of change in contact angle, SD, and R^2 are the standard deviation and coefficient of determination, respectively

than that of other types of biochar. This discrepancy may be attributable to variations in the components of feedstocks. A pH comparison of the 18 types of biochar revealed that the highest pH was observed in WS700 (10.54), while PN300 exhibited the lowest pH (5.99). FTIR analyses of 18 biochars (Fig. S1) revealed that biochars produced at lower pyrolysis temperatures possessed more abundant surface functional groups compared to those prepared at higher temperatures. Specifically, aromatic C=C bonds (1590–1610 cm^{-1}) and aliphatic CH_2 groups (2926, 2853,1450 and 1400 cm^{-1}) were detected across all pyrolysis temperatures; ester C=O groups (1670–1690 cm^{-1}) were distinctly observed in biochars pyrolyzed at low (300 °C) and intermediate (500 °C) temperatures; whereas carboxyl C=O groups (1315 cm^{-1}) were exclusively identified in low-temperature biochars. In addition, C–O–C moieties (1159–1175 cm^{-1})—characteristic functional groups of lignocellulose biomass-derived biochars—were universally detected across all biochars.

Among the 18 types of biochars studied, the highest and lowest CA_0 were found in PN300 (142.34°) and TP700 (86.60°), respectively (Table 3). For the majority of the biochars, the CA_0 values at lower pyrolysis temperatures were significantly higher ($p < 0.05$) than those at higher temperatures (Fig. S5). It suggests that, rather than high-temperature pyrolyzed biochar, the low-temperature pyrolyzed biochar is more hydrophobic. This phenomenon may be attributed to the pyrolysis of certain hydrophobic functional groups (e.g., $–CH_2$, Fig. S1) at elevated temperatures, leading to a reduction or complete disappearance of their characteristic peak intensities. Meanwhile, the C–O–C groups exhibit a certain degree of hydrophilicity. Correlation analysis revealed that the relative abundance of C–O–C groups increases with rising pyrolysis temperature (Table S6) and shows a negative correlation with CA_0 (Fig. S6), which indirectly confirms that biochars produced at lower pyrolysis temperatures have stronger hydrophobicity. It is worth mentioning that, similar to the standard materials, biochars exhibited contradictory results when assessing the hydrophobicity using WDPT and CA methods (Table 3). For example, in standard materials such as Fe sheet 100 and Fe sheet 200, as well as in biochars like CS500, CS700,

Table 2 Classification of hydrophobicity based on dynamic contact angle[a]

Group	Category	Hydrophobicity criterion	Examples in this study
i	Super hydrophobic	CA_0≧ 150° CA_90≈CA_0 (*n.s.*)	None
ii	Strongly hydrophobic	90° ≤ CA_0 < 150° CA_90≈CA_0 (*n.s.*)	Cu spheres 200 Cu dendriform 200 TiO_2 100 PS100 PP100 PTFE100 PE100 graphite 80–120
iii	'Pseudo' hydrophobic	90° ≤ CA_0 < 150° CA_90 < CA_0 ($p \leq 0.05$)	Fe sheet 100 Fe sheet 200 PA (66) 100 $CaSiO_3$ 200
iv	Hydrophilic	CA_0 < 90°	Fe spheres 100 Fe spheres 200 $Al_2O_3$100-200

[a] CA_0 and CA_90 present the contact angle measured at 0 s and 90 s, respectively; n.s. and $p \leq 0.05$ show that the CA_0 and CA_90 are not significantly and significantly different, respectively; Examples are the standard materials labelled the form of composition, shape, and mesh number

[b] **S**tandard materials are labelled as 'substance, shape, mesh number', whereas PS, PP, PTFE, PE, and PA (66) are the abbreviations for polystyrene, polypropylene, polytetrafluoroethylene, polyethylene, and nylon (66), respectively

TP500, PW700, and WS700, the WDPT results indicated hydrophilicity, while their CAs were > 90°, suggesting hydrophobicity. There was no significant difference between CA_90 and CA_0 for these biochars (Fig. 2). However, for six biochars- CS500, CS700, TP500, TP700, WS500, and WS700- the CA significantly decreased over time (Fig. 3, Table S5). According to surface properties in Table 2, most of these biochars were either 'pseudo'-hydrophobic or hydrophilic, considering ultimately hydrophilic in nature.

A gradual reduction in CA over time has been observed in previous studies (Chen et al. 2022; Hu et al. 2023; Wang et al. 2023), whereas transition has been observed even from > 90° to < 90° (Wu and Yang 2023; Xu et al. 2023). When investigating the permeation rate of surfactant into hydrophobic porous media, Ogunmokun and Wallach (2024) found that the CA of porous media decreased over time across all treatments, whereas the CA_0 value dropped from > 120° to around 90° in 30 s and finally dropped to about 70° within 300 s. The rearrangement and orientation of organic hydrophobic molecules on the porous media surface are crucial to explain the decrease in CA (Ogunmokun and Wallach 2024). Ivanova et al. (2023) observed that after 6 years of field trials, the CA of aged biochar decreased over time, reaching 0° after 20 s. In this case, the inherent heterogeneity of material surface structure resulted in spontaneous changes in CA. To summarize, the decline in CA could be attributed to either physical structure or the chemical components on material surface, however, the full scope of the influence requires further investigation and integration.

Based on our new hydrophobicity evaluation method, the hydrophobicity of 18 biochars fell into three out of four categories, with no super hydrophobic biochar observed. The classifications were as follows: Strongly hydrophobic biochar, e.g., CS300, TP300, PN300-700, PT300-700, PW300-700, and WS300; 'Pseudo'-hydrophobic biochar, e.g., WS500, WS700, CS500, CS700, and TP500; Hydrophilic biochar, e.g., TP700. According to this new method, the hydrophobicity of both strongly hydrophobic and hydrophilic biochar could be assessed by CA_90. Based on linear fitting (Fig. 3), when the slopes |k| values of CA were equal, e.g., CS500 vs CS700, WS700 vs TP500, then CA_90 should be used to differentiate their hydrophobicity. Consequently, the order of hydrophobicity was WS500 > CS700 > CS500 > WS700 > TP500. Correlation analysis indicated that most properties (pore volume, total carbon, specific surface area, and ash content) did not show any significant correlation with CA_90 or CA_0, whereas a strong negative correlation was observed between biochar pH and CA_0 ($r = -0.55$, $p = 0.017$, $n = 18$), and CA_90 ($r = -0.68$, $p = 0.002$, $n = 18$). This suggests that CA_0 and CA_90 tend to decrease with rising biochar pH. Furthermore, the relative abundance of surface functional groups on the biochar was also linked to CA_0 and CA_90. The functional group relative abundance was determined by the ratio of characteristic FTIR peak areas between paired functional groups (Mao et al. 2019). Both peak area ratios of aliphatic ($-CH_2$)/C=C and ester (–C=O)/C=C groups did not significantly correlate to either CA_0 or CA_90 of the biochar (Fig. S6). However, the ratio of the O–C–O/C=C

Table 3 WDPT and initial contact angle (CA_0) of 18 types of biochars

Biochar[a]	WDPT (s)	Hydrophobic level[b]	CA_0 (°)[c]
CS300	> 3600	Extremely hydrophobic	137.68 ± 2.63bc
CS500	2.65 ± 0.50	Hydrophilic	131.69 ± 4.42d
CS700	1.45 ± 0.40	Hydrophilic	131.68 ± 3.43d
TP300	> 3600	Extremely hydrophobic	139.46 ± 1.99abc
TP500	0.66 ± 0.122	Hydrophilic	90.16 ± 5.10g
TP700	0.55 ± 1.33	Hydrophilic	86.60 ± 3.44h
PW300	> 3600	Extremely hydrophobic	136.63 ± 4.26c
PW500	7.29 ± 1.65	Slightly hydrophobic	138.07 ± 3.23c
PW700	3.52 ± 1.12	Hydrophilic	127.70 ± 4.84f
PT300	> 3600	Extremely hydrophobic	136.94 ± 2.26c
PT500	> 3600	Extremely hydrophobic	136.94 ± 4.32bc
PT700	5.70 ± 0.68	Slightly hydrophobic	121.73 ± 4.57e
PN300	> 3600	Extremely hydrophobic	142.34 ± 1.11a
PN500	> 3600	Extremely hydrophobic	140.93 ± 2.75ab
PN700	110.44 ± 80.27	Strongly hydrophobic	142.13 ± 2.45a
WS300	1887.22 ± 180.61	Severely hydrophobicity	140.63 ± 2.96ab
WS500	38.51 ± 9.76	Slightly hydrophobic	136.66 ± 1.99c
WS700	3.08 ± 0.44	Hydrophilic	136.32 ± 3.06c

[a] Biochar is labelled as biomass and pyrolysis temperature; where CS, TP, PT, PW, PN, WS represented the biomasses of cotton stalk, tangerine peel, poplar wood sawdust, pine wood sawdust, pine needle, and wheat straw, respectively

[b] Hydrophobic level here was determined by WDPT method (Bisdom et al. 1993)

[c] Lowercase letters indicate significant differences of CA_0 among the various types of biochars ($p \leq 0.05$)

group was significantly negatively correlated with CA_0 (r = −0.49, $p = 0.039$, n = 18). For CA_90, significant negative correlations were observed for both the C–O–C/C=C (r = −0.50, $p = 0.034$, n = 18) and O–C=O/C=C (r = −0.55, $p = 0.019$, n = 18) functional groups. It demonstrated that relatively higher abundance of carboxyl groups (O–C=O) and ether groups (C–O–C) correlate with stronger hydrophilicity. This aligns with the consensus in most studies as carboxyl groups are strongly hydrophilic (Rechberger et al. 2017; Watson et al. 2021; Zhang et al. 2025), while ether groups are also recognized as hydrophilic functional groups (Kravchenko et al. 2024). By conducting a correlation analysis between CA_0 and CA_90, it was found that CA_90 can provide a more comprehensive assessment of water repellency. This further validates the rationality of the DCA method.

3.5 Effects of biochar on soil water repellency

The control group of soil exhibited non-water-repellency throughout the 90-day period (CA_0 < 90°, WDPT < 5 s). Upon initial incorporation of biochar, an addition rate of 1% was sufficient to transform non-water-repellent soils (CA_0 < 90°) into water repellent (CA_0 > 90°), significantly increasing SWR (Fig. S7). Similar trends were observed at the 5% addition rate, although the performance of TP500 and TP700 was less pronounced. In general, the addition of most biochars notably enhanced the water repellency of non-water-repellent soils. It is worth noting that higher biochar addition rates resulted in greater increases in CA_0 (CA_0 > 120°) (Kinney et al. 2012; Mao et al. 2019; Ebrahimzadeh Omran et al. 2020; Liu et al. 2022). Xu et al. (2023) investigated the water characteristics of sandy soil amended with hydrochar derived from food waste, and found that higher addition rate increased SWR, though this effect diminished over time. Similarly, Shahsavar et al. (2024) indicated that the addition rate of biochar significantly affects SWR. These findings suggest that the biochar addition can induce SWR.

Regarding WDPT, at a 1% addition rate, only CS300 and PN300 exhibited notable increases in penetration time (Fig. S8), although the soils remained non-water-repellent (WDPT < 5 s). At a 5% addition rate, CS300, PN300, PN500, and WS300 markedly extended the infiltration time, with all but PN300 transitioning the soil from non-water-repellent to water repellent states (WDPT > 5 s). However, after 90 days of incubation, the effectiveness of most biochars gradually declined (Fig. S6). This finding aligns with the observations reported by Ojeda et al. (2024) who identified this following a 1-year period of soil mixed with biochar. The reduction in SWR during incubation may be attributed to multiple mechanisms. Firstly, prolonged incubation induces aging-mediated surface oxidation of biochar, facilitating its transformation from water repellent to non-water-repellent particles (Ge et al. 2024). Additionally, fungal regrowth promotes non-water-repellency through preferential degradation of hydrophobic compounds (Boak et al. 2025). Furthermore, certain bacterial strains contribute to SWR reduction via hydrocarbon removal or utilization of hydrocarbons as energy substrates for growth and reproduction (Ali et al. 2023). At the 1% addition rate, the impacts of CS and PW biochars were negligible, while PN300 significantly increased infiltration time without altering the soil's non-water-repellency (Fig. S8).

The DCA method confirmed that the original soil was non-water-repellent (Fig. 4), consistent with the CA_0 and WDPT findings. At an addition rate of 1%, regardless of incubation duration, most biochars increased the soil DCA within 90 s when compared to the control group, although the CA_90 remained below 90°. At a 5% addition rate, the increase in CA was more pronounced than that observed at a 1% addition rate, as evident from the upward shift of the curve. Despite these increases, the soil's non-water-repellent nature remained unchanged, resulting in a 'pseudo'-water-repellent state. To evaluate

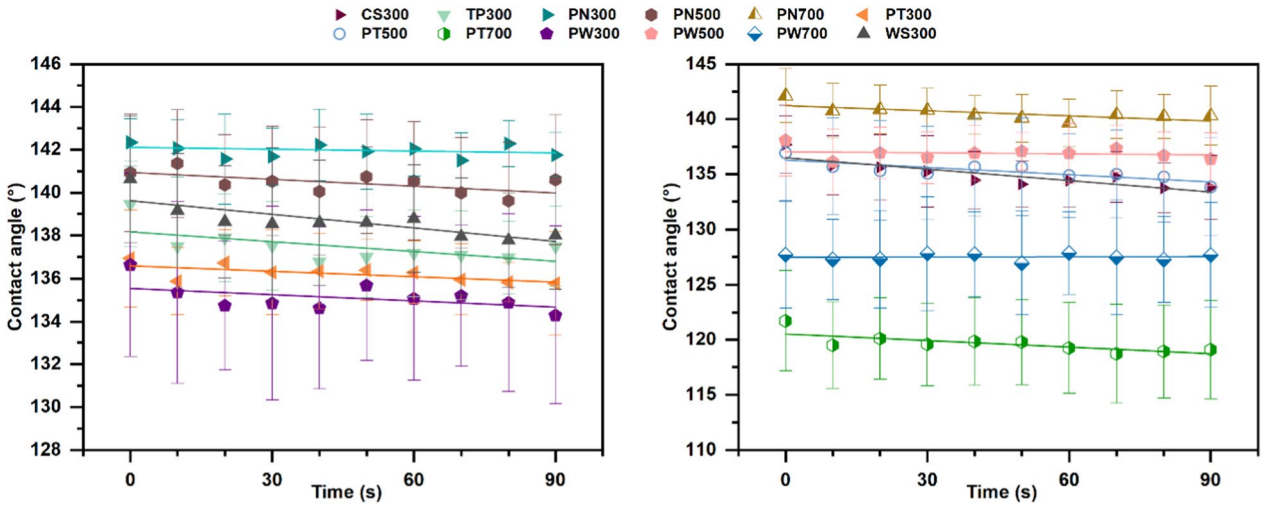

Fig. 2 Contact angle of biochars changed within 90 s, where no significant difference was found between the contact angle at 90 s and the initial contact angle. Biochar was labelled as 'biomass, pyrolysis temperature', where CS, TP, PT, PW, PN, and WS stand for cotton stalk, tangerine peel, poplar wood sawdust, pine wood sawdust, pine needle, and wheat straw, respectively

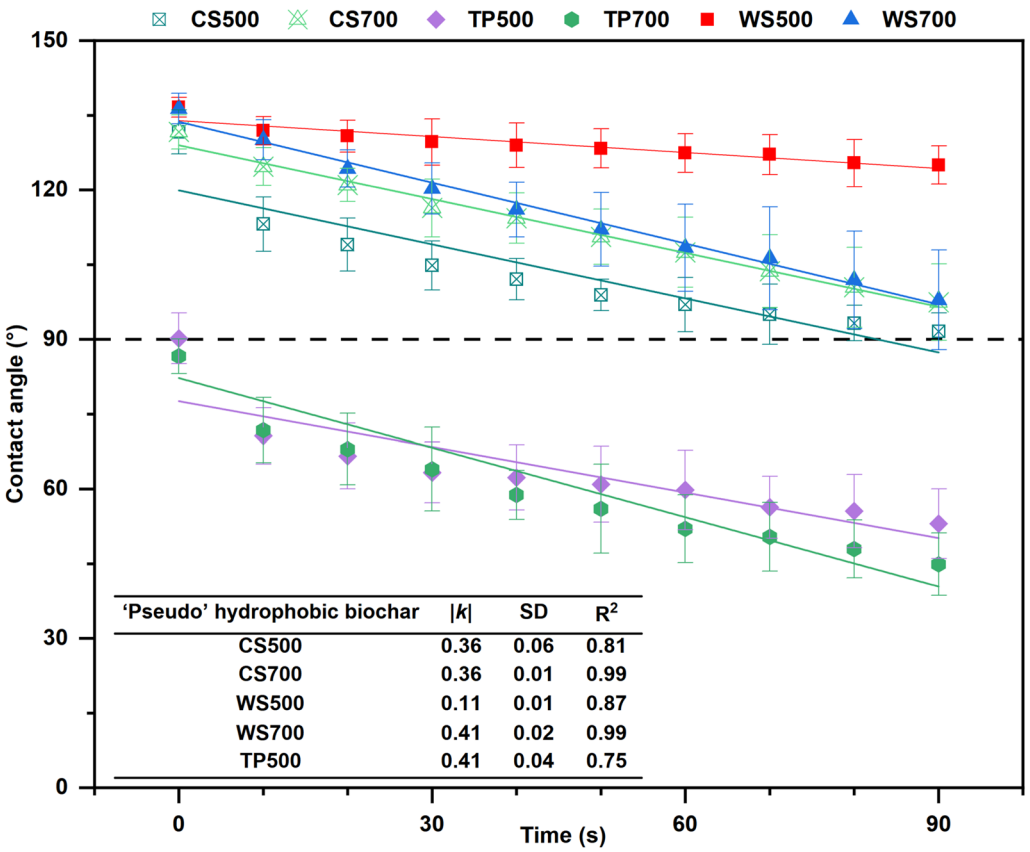

Fig. 3 The contact angle of 'pseudo'-hydrophobic biochar (CS500, CS700, WS500, WS700, and TP500) and hydrophilic biochar (TP700) significantly decreased in 90 s. Biochar was labelled as 'biomass, pyrolysis temperature', where CS, TP, and WS stand for cotton stalk, tangerine peel and wheat straw, respectively. $|k|$ represents the slope of linear fitting, meaning the rate of change in contact angle, SD and R^2 are the standard deviation and coefficient of determination, respectively

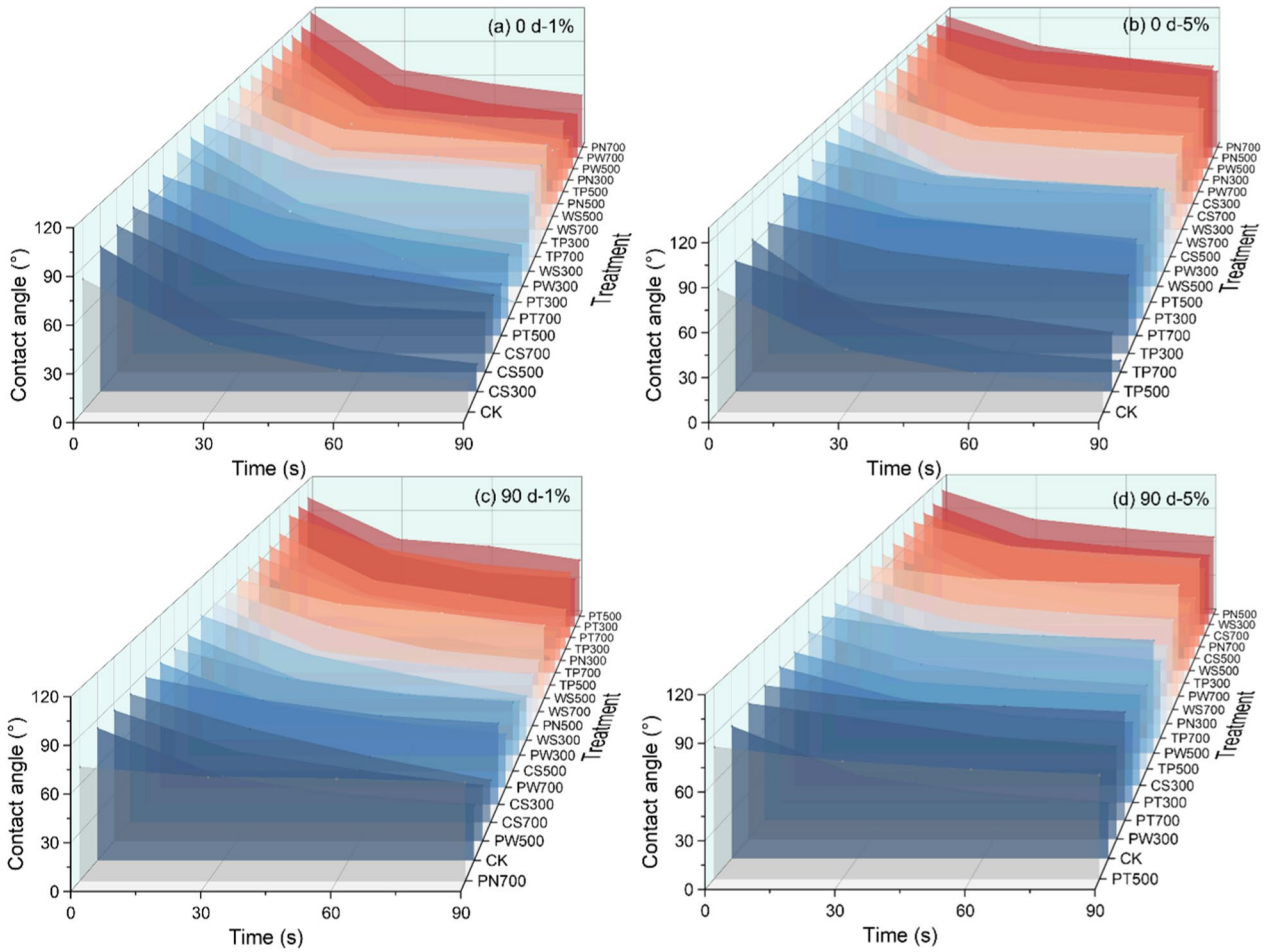

Fig. 4 Dynamic change in contact angle (CA) of biochar-amended soil within 90 s. **a** and **b** show the CA of soil with 1% and 5% biochar addition rate at day 0, respectively, **c** and **d** show the CA of soil with 1% and 5% biochar addition rate at day 90, respectively. The dashed line represents the case where CA = 90°. Biochar was labelled as 'biomass, pyrolysis temperature', where CS, TP, PT, PW, PN and WS stand for cotton stalk, tangerine peel, poplar wood sawdust, pine wood sawdust, pine needle, and wheat straw, respectively

the influence of biochar hydrophobicity on SWR, a comparative analysis was conducted. The CA_90 of soil amended with biochar were juxtaposed against those of the control soil (as depicted in Fig. 5). Before and after incubation, the most biochar-amended soil showed positive ΔCA_90, demonstrating the increment of SWR owing to biochar addition (Mao et al. 2019; Liu et al. 2022). For the soil amended with 5% biochar, on day 0, the ΔCA_90 of both CS and WS biochar-added soils exhibited a gradual decrease as the pyrolysis temperature increased, however, after a 90d incubation, the decreasing tendency was not observed. Compared to other biochars, CS and WS biochars exhibited 'pseudo'-water-repellency (Fig. 3), additionally, the ΔCA_0 of soil, but not ΔCA_90, showed a significant correlation with the CA_90 of biochar ($p < 0.001$) (Fig. 6). Taken together, these results reveal that the effect of 'pseudo'-water-repellent biochar on SWR may be influenced by biochar-water interaction during incubation. Furthermore, the 'pseudo'-water-repellent nature of biochar could potentially increase the complexity of predicting its effects on soil hydrological properties. These findings suggest that the efficacy of biochar in modifying SWR is influenced by both addition rate and incubation duration. The original hydrophobicity of biochar may offer a practical approach for the regulation of SWR across different incubation conditions and timeframes.

3.6 Paradoxical phenomena of CA and WDPT

The discrepancies in water repellency determination between CA and WDPT measurements have been discussed in previous studies, for instance, Ewa et al. found the CA of soil ranged from 40° to 90°, with the WDPT exceeding 5 s (Papierowska et al. 2018). By analyzing the CA and WDPT of 17 standard materials and 18 biochars, this study observed a typical paradoxical phenomenon in

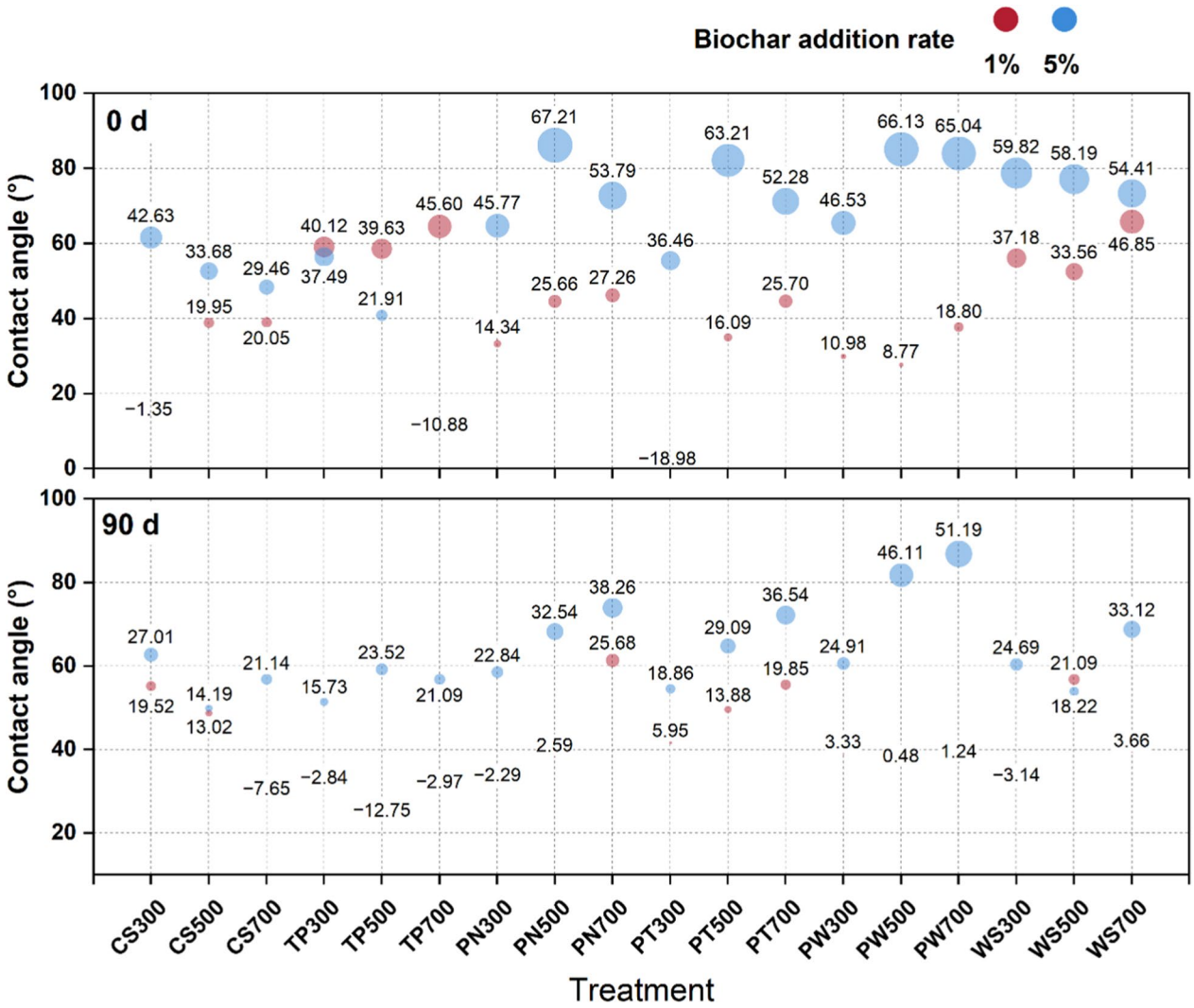

Fig. 5 The difference of contact angle at 90 s (ΔCA_90) between biochar-amended soil and control soil after 0 and 90 days of incubation. The X-label presents the soil amended with different types of biochar. The dashed line represents the case where the CA_90 of CK. The values in the figure represent the differences between the biochar and the control soil CA_90. Different colors represent different addition rates. Biochar was labelled as 'biomass, pyrolysis temperature', where CS, TP, PT, PW, PN and WS stand for cotton stalk, tangerine peel, poplar wood sawdust, pine wood sawdust, pine needle, and wheat straw, respectively

both standard materials (Fe sheet 100 and Fe sheet 200) and biochar (TP500, CS500, CS700, WS700). Generally, while the WDPT showed hydrophilicity (WDPT < 5 s), the CA_0 results indicated hydrophobicity (CA_0 > 90 s). For these six materials, hydrophobicity may be overestimated if evaluated solely based on CA_0. When the dynamic contact angle (DCA) method was applied, the droplets dispersed on the material surface and their CA_90 were significantly lower than CA_0. These materials were categorized as 'pseudo'-hydrophobic. The DCA method provided a more accurate evaluation of actual hydrophobicity of materials, reconciling the discrepancies between CA_0 and WDPT measurements (Fig. 6). For instance, the WDPT of CS500 was 2.65 s, classifying it as hydrophilic, while its CA_0 was 131.69°, suggesting strong hydrophobicity. However, CS500 was classified as 'pseudo'-hydrophobic (rate of CA change $|k| > 0$) based on our DCA evaluation method, aligning with the WDPT measurement. In summary, the combination of DCA method and the newly introduced 'pseudo'-hydrophobicity concept has been demonstrated in our study to overcome the inconsistency in hydrophobicity assessment by CA_0 and WDPT measurements.

By comparing the CA_0 and WDPT of biochar-added soil, it is evident that at the onset of incubation, the CA_0 of soil amended with biochar exceeded 90°, indicating

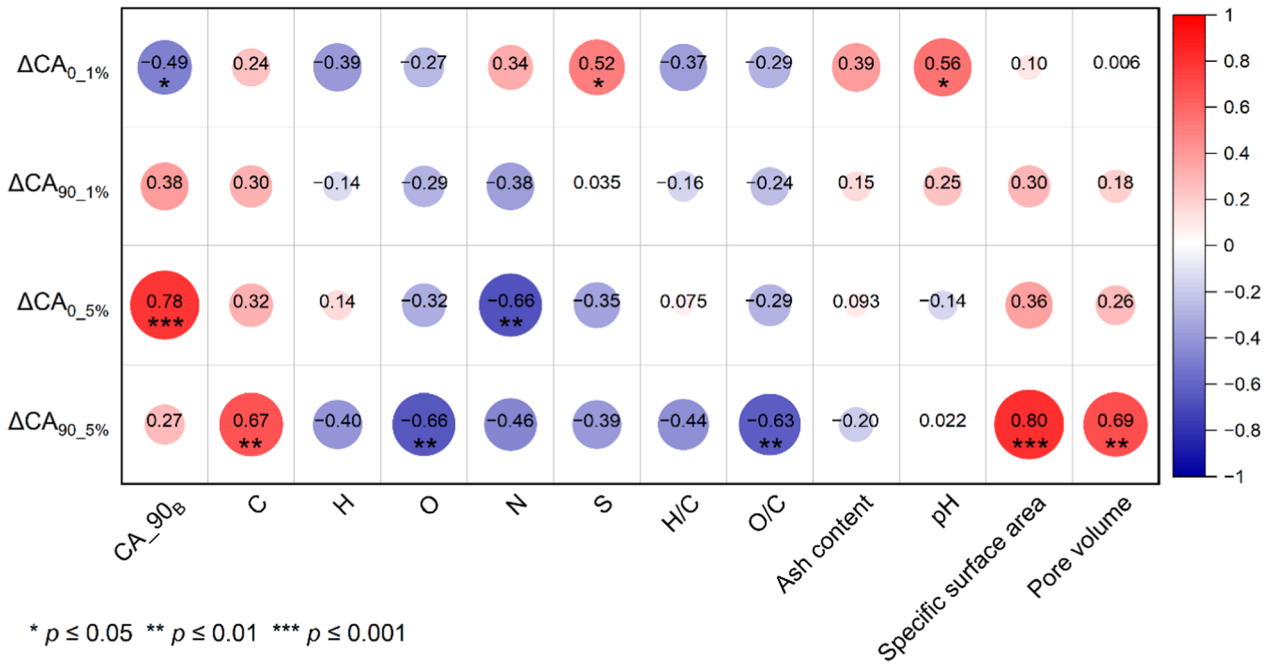

Fig. 6 Correlation analysis between ΔCA_90 of biochar-amended soil and biochar properties. The numbers in the circle represent the correlation coefficient. ΔCA_90 refers to the difference between the contact angle at 90 s (CA_90) of the biochar-amended soil and the control soil after incubation, ΔCA_{0}_1% presents the ΔCA_90 at day 0 of soil with 1% biochar addition rate, and CA_90_{B} represents the CA_90 of biochar

water repellency (Fig. S7). However, WDPT measurements revealed that only soil with a 5% biochar addition rate (CS300, PN500, and WS300) exhibited water repellency (WDPT > 5 s) (Fig. S8). Over the 90d incubation, the influence of biochar on soil SWR diminished, with a notable reduction in the occurrence of discrepancies between CA_0 and WDPT results. However, they remained prevalent, particularly for the 5% addition rate treatments (Fig. S7, S8). Further analysis using DCA (Fig. 4) confirmed that the addition of 18 different biochars did not alter the non-water-repellent nature of the soil. This conclusion is consistent with 97.5% of the WDPT results.

Methods for assessing water repellency exhibit distinct advantages and limitations. WDPT method, despite its significant limitations in testing procedures—it only provides an indirect assessment of water repellency (Bachmann et al. 2000; Leelamanie et al. 2008) and is susceptible to operator subjectivity due to the complete encapsulation of water droplets by heterogeneous surfaces under surface tension (Liu et al. 2022; Veneris and Farid 2024). The sessile drop method is commonly employed to determine the wettability of solid surfaces, where repeatable advancing contact angles (ACA) and receding contact angles (RCA) can be achieved by controlling changes in the volume of the probe liquid. However, such measurement typically takes 15–20 min to complete, and the entire experimental process, including replicated experiments, can require 1 to 2 h (Huhtamäki et al. 2018). Time-lapse sessile drop measurements are more commonly applied in analyses of surface wetting dynamics, primarily involving investigations into evaporation, viscosity, and absorption effects (Hu and Larson 2002; Wu et al. 2025). Using CA_0 can capture instantaneous repellency, while it may fail to entirely reflect the droplet diffusion. Therefore, building upon CA_0, the DCA method is proposed to simultaneously account for changes in hydrophobicity over time. Consequently, the DCA method has a broader scope of application while maintaining a high level of accuracy.

Overall, this paradoxical phenomenon was observed across three distinct material types in this study, encompassing standard materials, biochars, and soils, and its frequency increased with the complexity of the subjects. The results obtained through the DCA method exhibit a high degree of consistency with those derived from the WDPT, thereby effectively addressing contradictions in the findings (Fig. 7).

4 Conclusions

Understanding the level of biochar hydrophobicity is crucial for predicting its interactions with water, influencing its application in environmental protection, agriculture, and material science. Current methods for

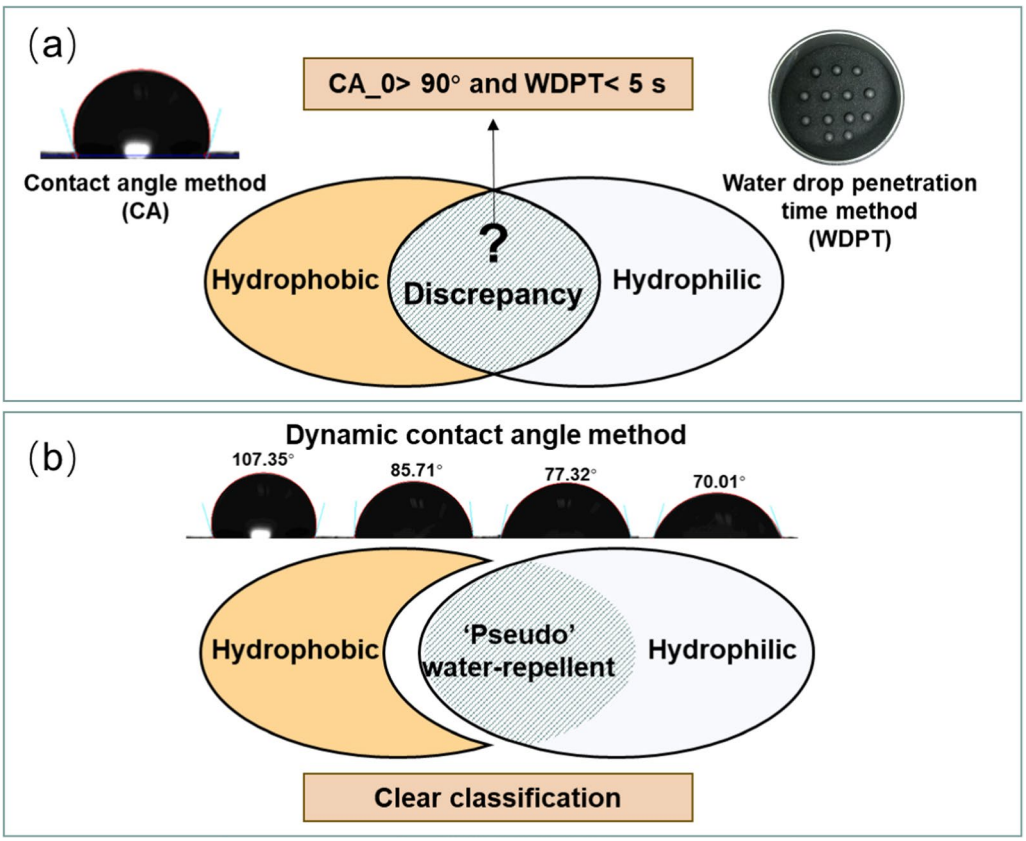

Fig. 7 **a** Inconsistences in assessing biochar hydrophobicity between contact angle and water drop penetration time resulted in overlapped classification; **b** The addition of dynamic contact angle method and the introduction of 'pseudo'-hydrophobicity clearly distinguished between hydrophobic and hydrophilic materials

evaluating hydrophobicity, based on principles of CA and droplet penetration, are widely used. However, discrepancies observed between CA and WDPT measurements underscore the need for a multidimensional approach to accurately assess biochar hydrophobicity. This study highlighted the temporal inconsistencies between these two methods and proposed a novel approach using DCA measurement to reconcile these discrepancies. DCA can represent the diffusion of water droplets in alignment with water penetration time. In conjunction with DCA, a new classification was established by first defining 'pseudo'-hydrophobicity. 'Pseudo'-hydrophobicity means that the CA of hydrophobic solid surface drops below 90° within 90 s once the water droplet diffuses on its surface. This approach clearly demonstrated a decrease in CA over time and the transition from hydrophobic surface to hydrophilic surface. This new concept was validated for both standard Fe sheets and mid and high temperature biochars, where original hydrophilic materials could be inaccurately considered as hydrophobic if their CA_0 was solely considered. The combination of CA_90 and rate of change in CA over time ($|k|$) is suggested as the new criterion for hydrophobicity evaluation, particularly for 'pseudo'-hydrophobic materials. Furthermore, the DCA method was employed to evaluate SWR at different addition rates and incubation periods. While CA_0 indicated that biochar could significantly induce hydrophobicity, the DCA indicated that the incubated soil remained in a 'pseudo'-hydrophobic state, retaining its fundamental hydrophilic nature, which is consistent with WDPT measurements.

Although our study used a 90-s observation period for the DCA method, the primary contribution lies not in the specific duration but in introducing a novel perspective on the temporal dynamics of CA. This approach addresses ambiguities in defining the actual hydrophobicity, particularly for materials like biochar, where water droplets may diffuse over time. We propose that water droplet diffusion should be considered a critical factor in hydrophobicity across various disciplines, including environmental science, agriculture, and materials science. In the future, by using the DCA method to deepen the understanding of SWR, it will promote the large-scale

application of biochar in improving soil water retention, achieving multiple benefits, including water conservation, yield increases, ecological restoration, and vegetation recovery. It is particularly important to emphasize that the agricultural and forestry wastes should be rationally utilized as feedstock of biochar. This approach effectively circumvents ethical concerns such as competition with food production. Our DCA method provides a more accurate and comprehensive framework for the evaluation of water repellency.

Abbreviations

CA	Contact angle
CA_0	Initial contact angle
CA_90	Contact angle at 90 s
WDPT	Water drop penetration time
PS	Polystyrene
PP	Polypropylene
PTFE	Polytetrafluoroethylene
PP	Polypropylene
PA (66)	Nylon (66)
WS	Wheat straw
CS	Cotton stalk
PW	Pine wood sawdust
PT	Poplar wood sawdust
PN	Pine needles
TP	Tangerine peels

Supplementary Information

The online version contains supplementary material available at https://doi.org/10.1007/s42773-025-00555-y.

Supplementary material 1.

Acknowledgements
We would like to thank the Tianshan Talent Training Program, the Key Research and Development Program of Xinjiang Uygur Autonomous Region and the Natural Science Foundation of Xinjiang Uygur Autonomous Region. We would like to express our gratitude to the Fukang National Field Scientific Observation and Research Station for Desert Ecosystems for their assistance during the soil and biomass sampling.

Author contributions
All authors contributed to the study's conception and design. Material preparation, data collection, and analysis were performed by Wei Jing, Kai Yang, Qilin Kang, Yaoming Li, and Wei Li. Mingjie Su was responsible for the FTIR analyses of 18 types of biochar and the analysis of functional groups. Supervision and funding acquisition were provided by Kun Zhang and Jiefei Mao. The first draft of the manuscript was written by Wei Jing, and all authors commented on previous versions of the manuscript. All authors read and approved the final manuscript.

Funding
This study was funded by the Tianshan Talent Training Program (Grant Number 2023TSYCCX0080), the Key Research and Development Program of Xinjiang Uygur Autonomous Region (Grant Number 2023B02002), and the Natural Science Foundation of Xinjiang Uygur Autonomous Region (Grant Number 2021D01C048).

Data availability
The datasets used or analyzed during the current study are available from the corresponding author upon reasonable request.

Declarations

Competing interests
The authors declare that the research was conducted in the absence of any commercial or financial relationships that could be construed as a potential competing interest.

Author details
[1]State Key Laboratory of Ecological Safety and Sustainable Development in Arid Lands, Xinjiang Institute of Ecology and Geography, Chinese Academy of Sciences, Urumqi 830011, China. [2]College of Ecology and Environment, Xinjiang University, Urumqi 830017, China. [3]Xinjiang Vocational and Technical College of Construction, Urumqi 830054, China. [4]Key Laboratory of Oasis Ecology of Education Ministry, Urumqi 830017, China. [5]Research Center for Ecology and Environment of Central Asia, Chinese Academy of Sciences, Urumqi 830011, China. [6]University of Chinese Academy of Sciences, Beijing 100049, China.

Received: 17 February 2025 Revised: 22 October 2025 Accepted: 3 December 2025
Published online: 01 February 2026

References

Acharya BS, Dodla S, Wang JJ, Pavuluri K, Darapuneni M, Dattamudi S, Maharjan B, Kharel G (2024) Biochar impacts on soil water dynamics: knowns, unknowns, and research directions. Biochar 6:34. https://doi.org/10.1007/s42773-024-00323-4

Adhikari S, Timms W, Mahmud MAP (2022) Optimising water holding capacity and hydrophobicity of biochar for soil amendment – a review. Sci Total Environ 851:158043. https://doi.org/10.1016/j.scitotenv.2022.158043

Albalasmeh AA, Mohawesh OE (2023) Effects of olive mill wastewater on soil physical and hydraulic properties: a review. Water Air Soil Pollut 234:42. https://doi.org/10.1007/s11270-022-06055-0

Alghamdi AG, Alkhasha A, Ibrahim HM (2020) Effect of biochar particle size on water retention and availability in a sandy loam soil. J Saudi Chem Soc 24:1042–1050. https://doi.org/10.1016/j.jscs.2020.11.003

Ali MH, Khan MI, Naveed M, Tanvir MA (2023) Microbe-assisted rhizoremediation of hydrocarbons and growth promotion of chickpea plants in petroleum hydrocarbons-contaminated soil. Sustainability 15:6081. https://doi.org/10.3390/su15076081

Aranda V, Calero J, Plaza I, Ontiveros-Ortega A (2016) Long-term effects of olive mill pomace co-compost on wettability and soil quality in olive groves. Geoderma 267:185–195. https://doi.org/10.1016/j.geoderma.2015.12.027

Bachmann J, Horton R, Van Der Ploeg RR, Woche S (2000) Modified sessile drop method for assessing initial soil-water contact angle of sandy soil. Soil Sci Soc Am J 64:564–567. https://doi.org/10.2136/sssaj2000.642564x

Baiamonte G, Crescimanno G, Parrino F, De Pasquale C (2019) Effect of biochar on the physical and structural properties of a sandy soil. CATENA 175:294–303. https://doi.org/10.1016/j.catena.2018.12.019

Bisdom EBA, Dekker LW, Schoute JFT (1993) Water repellency of sieve fractions from sandy soils and relationships with organic material and soil structure. Geoderma 56:105–118. https://doi.org/10.1016/0016-7061(93)90103-r

Boak EN, Bowen BP, Louie KB, Northen TR, Kroeger ME (2025) Bacterial and fungal composition and exometabolites control the development and persistence of soil water repellency. ISME Commun 5:ycaf084. https://doi.org/10.1093/ismeco/ycaf084

Buczko U, Bens O (2006) Assessing soil hydrophobicity and its variability through the soil profile using two different methods. Soil Sci Soc Am J 70:718–727. https://doi.org/10.2136/sssaj2005.0183

Cervera-Mata A, Aranda V, Ontiveros-Ortega A, Comino F, Martín-García JM, Vela-Cano M, Delgado G (2021) Hydrophobicity and surface free energy to assess spent coffee grounds as soil amendment. Relationships with soil quality. CATENA 196:104826. https://doi.org/10.1016/j.catena.2020.104826

Chau HW, Biswas A, Vujanovic V, Si BC (2014) Relationship between the severity, persistence of soil water repellency and the critical soil water content

in water repellent soils. Geoderma 221:113–120. https://doi.org/10.1016/j.geoderma.2013.12.025
Chen KW, Sun FZ, Liu ZT, Peng H, Jiang JL, Lyu JX et al (2022) Orthotropic wetting dynamics of wood: trade-off between surface spreading and penetration. Eur J Wood Wood Prod 80:669–679. https://doi.org/10.1007/s00107-021-01780-5
DeBano LF (2000) Water repellency in soils: a historical overview. J Hydrol 231–232:4–32. https://doi.org/10.1016/S0022-1694(00)00180-3
Ding YB, Gong XL, Xing ZX, Cai HJ, Zhou ZQ, Zhang DD et al (2021) Attribution of meteorological, hydrological and agricultural drought propagation in different climatic regions of China. Agric Water Manage 255:106996. https://doi.org/10.1016/j.agwat.2021.106996
Doerr SH, Shakesby RA, Walsh RPD (1998) Spatial variability of soil hydrophobicity in fire-prone eucalyptus and pine forests, Portugal. Soil Sci 163:313–324. https://doi.org/10.1097/00010694-199804000-00006
Doerr SH, Shakesby RA, Walsh RPD (2000) Soil water repellency: its causes, characteristics and hydro-geomorphological significance. Earth Sci Rev 51:33–65. https://doi.org/10.1016/S0012-8252(00)00011-8
Ebrahimzadeh Omran S, Shorafa M, Zolfaghari AA, Toolarood AAS (2020) The effect of biochar on severity of soil water repellency of crude oil-contaminated soil. Environ Sci Pollut Res 27:6022–6032. https://doi.org/10.1007/s11356-019-07246-9
Fu Q, Zhao H, Li H, Li TX, Hou RJ, Liu D, Ji Y, Gao Y, Yu PF (2019) Effects of biochar application during different periods on soil structures and water retention in seasonally frozen soil areas. Sci Total Environ 694:133732. https://doi.org/10.1016/j.scitotenv.2019.133732
Ge M, Wang BY, Chen BF, Xie HF, Sun HJ, Sun K, Feng YF (2024) Hydrochar and its dissolved organic matter aged in a 30-month rice-wheat rotation system: do primary aging factors alter at different stages? Environ Sci Technol 58:3019–3030. https://doi.org/10.1021/acs.est.3c08044
Gray M, Johnson MG, Dragila MI, Kleber M (2014) Water uptake in biochars: the roles of porosity and hydrophobicity. Biomass Bioenergy 61:196–205. https://doi.org/10.1016/j.biombioe.2013.12.010
Griffo R, Di Natale F, Minale M, Sirignano M, Parisi A, Carotenuto C (2024) Analysis of carbon nanoparticle coatings via wettability. Nanomaterials 14:301. https://doi.org/10.3390/nano14030301
Haddad SA, Mowrer J, Thapa B (2022) Biochar and compost from cotton residues inconsistently affect water use efficiency, nodulation, and growth of legumes under arid conditions. J Environ Manage 307:114558. https://doi.org/10.1016/j.jenvman.2022.114558
Hallett PD, Baumgartl T, Young IM (2001) Subcritical water repellency of aggregates from a range of soil management practices. Soil Sci Soc Am J 65:184–190. https://doi.org/10.2136/sssaj2001.651184x
Hewelke E, Zaniewski PT, Zaniewska E, Papierowska E, Gozdowski D, Lachacz A, Górska EB (2023) Does spontaneous secondary succession contribute to the drying of the topsoil? Forests 14:356. https://doi.org/10.3390/f14020356
Hu H, Larson RG (2002) Evaporation of a sessile droplet on a substrate. J Phys Chem B 106:1334–1344. https://doi.org/10.1021/jp0118322
Hu YC, Gan MX, Xie YM, Yu YS, Feng QH (2023) Facile fabrication of biometric cellulose-based films with superhydrophobicity and tunable optical performance. Appl Surface Sci 637:157924. https://doi.org/10.1016/j.apsusc.2023.157924
Huhtamäki T, Tian X, Korhonen JT, Ras RHA (2018) Surface-wetting characterization using contact-angle measurements. Nat Protoc 13:1521–1538. https://doi.org/10.1038/s41596-018-0003-z
Inyang M, Gao B, Yao Y, Xue YW, Zimmerman AR, Pullammanappallil P, Cao XD (2012) Removal of heavy metals from aqueous solution by biochars derived from anaerobically digested biomass. Bioresour Technol 110:50–56. https://doi.org/10.1016/j.biortech.2012.01.072
Ivanova N, Obaeed GLO, Sulkarnaev F, Buchkina N, Gubin A, Yurtaev A (2023) Effect of biochar aging in agricultural soil on its wetting properties and surface structure. Biochar 5:75. https://doi.org/10.1007/s42773-023-00272-4
Kinney TJ, Masiello CA, Dugan B, Hockaday WC, Dean MR, Zygourakis K, Barnes RT (2012) Hydrologic properties of biochars produced at different temperatures. Biomass Bioenerg 41:34–43. https://doi.org/10.1016/j.biombioe.2012.01.033
Kravchenko E, Dela Cruz TL, Sushkova S, Rajput VD (2024) Effect of wood and peanut shell hydrochars on the desiccation cracking characteristics of clayey soils. Chemosphere 358:142134. https://doi.org/10.1016/j.chemosphere.2024.142134
Leelamanie DAL, Karube J (2009) Time dependence of contact angle and its relation to repellency persistence in hydrophobized sand. Soil Sci Plant Nutr 55:457–461. https://doi.org/10.1111/j.1747-0765.2009.00387.x
Leelamanie DAL, Karube J, Yoshida A (2008) Relative humidity effects on contact angle and water drop penetration time of hydrophobized fine sand. Soil Sci Plant Nutr 54:695–700. https://doi.org/10.1111/j.1747-0765.2008.00296.x
Li Y, Ren X, Hill R, Malone R, Zhao Y (2018) Characteristics of water infiltration in layered water-repellent soils. Pedosphere 28:775–792. https://doi.org/10.1016/S1002-0160(17)60414-4
Liu Z, Ogunmokun FA, Wallach R (2022) Does biochar affect soil wettability and flow pattern? Geoderma 417:115826. https://doi.org/10.1016/j.geoderma.2022.115826
Mao JF, Zhang K, Chen BL (2019) Linking hydrophobicity of biochar to the water repellency and water holding capacity of biochar-amended soil. Environ Pollut 253:779–789. https://doi.org/10.1016/j.envpol.2019.07.051
Monroe J, Barry M, DeStefano A, Gokturk PA, Jiao S, Robinson-Brown D, Webber T, Crumlin EJ, Han S, Shell MS (2020) Water structure and properties at hydrophilic and hydrophobic surfaces. Annu Rev Chem Biomol 11:523–557. https://doi.org/10.1146/annurev-chembioeng-120919-114657
Muema FM, Richardson Y, Keita A, Sawadogo M (2024) An interdisciplinary overview on biochar production engineering and its agronomic applications. Biomass Bioenerg 190:107416. https://doi.org/10.1016/j.biombioe.2024.107416
Müller K, Carrick S, Meenken E, Clemens G, Hunter D, Rhodes P, Thomas S (2016) Is subcritical water repellency an issue for efficient irrigation in arable soils? Soil Tillage Res 161:53–62. https://doi.org/10.1016/j.still.2016.03.010
Ogunmokun FA, Wallach R (2024) Effect of surfactant surface and interfacial tension reduction on infiltration into hydrophobic porous media. Geoderma 441:116735. https://doi.org/10.1016/j.geoderma.2023.116735
Ojeda G, Gil JM, Mattana S, Bachmann J, Quenea K, Sobral AJFN (2024) Biochar ageing effects on soil respiration biochar wettability and gaseous CO_2 adsorption. Mitig Adapt Strateg Glob Change 29:11. https://doi.org/10.1007/s11027-024-10107-7
Papierowska E, Matysiak W, Szatyłowicz J, Debaene G, Urbanek E, Kalisz B, Łachacz A (2018) Compatibility of methods used for soil water repellency determination for organic and organo-mineral soils. Geoderma 314:221–231. https://doi.org/10.1016/j.geoderma.2017.11.012
Paz SM, Alberto LL, Rafael V, Lautaro BG, Alejandra MVC, Nirvana C, Guillermo PN, Germán SC (2024) Soil water repellency under Eucalyptus stands of different age and its relationship with soil hydrological function and soil organic matter. CATENA 246:108441. https://doi.org/10.1016/j.catena.2024.108441
Rechberger MV, Kloss S, Rennhofer H, Tintner J, Watzinger A, Soja G, Lichtenegger H, Zehetner F (2017) Changes in biochar physical and chemical properties: accelerated biochar aging in an acidic soil. Carbon 115:209–219. https://doi.org/10.1016/j.carbon.2016.12.096
Roberts KG, Gloy BA, Joseph S, Scott NR, Lehmann J (2010) Life cycle assessment of biochar systems: estimating the energetic, economic, and climate change potential. Environ Sci Technol 44:827–833. https://doi.org/10.1021/es902266r
Saha R, Galagedara L, Thomas R, Nadeem M, Hawboldt K (2020) Investigating the influence of biochar amendment on the physicochemical properties of podzolic soil. Agriculture 10:471. https://doi.org/10.3390/agriculture10100471
Santos JA, Gonzaga MIS, dos Santos WM, da Silva AJ (2022) Water retention and availability in tropical soils of different textures amended with biochar. CATENA 219:106616. https://doi.org/10.1016/j.catena.2022.106616
Schlaepfer DR, Bradford JB, Lauenroth WK, Munson SM, Tietjen B, Hall SA, Wilson SD, Duniway MC, Jia GS, Pyke DA, Lkhagva A, Jamiyansharav K (2017) Climate change reduces extent of temperate drylands and intensifies drought in deep soils. Nat Commun 8:14196. https://doi.org/10.1038/ncomms14196
Seitz S, Teuber S, Geißler C, Goebes P, Scholten T (2020) How do newly-amended biochar particles affect erodibility and soil water movement? - a small-scale experimental approach. Soil Syst 4:60. https://doi.org/10.3390/soilsystems4040060

Shahsavar AM, Mosaddeghi MR, Rahimmalek M, Gheysari M (2024) Interactive effects of wood biochar application and *Thymus* species on soil physical quality in irrigated farming. Soil till Re 244:106260. https://doi.org/10.1016/j.still.2024.106260

Tian YP, Yan SJ, Song CL, Wang CY, Chen J (2022) Research on the influence of micro-morphology on the hydrophobicity of material surface. Colloid Interface Sci Commun 46:100556. https://doi.org/10.1016/j.colcom.2021.100556

Usevičiūtė L, Baltrėnaitė E (2020) Methods for determining lignocellulosic biochar wettability. Waste Biomass Valoriz 11:4457–4468. https://doi.org/10.1007/s12649-019-00713-x

Veneris M, Farid A (2024) Finer measurement scales for induced hydrophobicity using the water droplet penetration test. Geotechnics 4(2):581–603. https://doi.org/10.3390/geotechnics4020032

Villagra-Mendoza K, Horn R (2018) Effect of biochar addition on hydraulic functions of two textural soils. Geoderma 326:88–95. https://doi.org/10.1016/j.geoderma.2018.03.021

Wang ZF, Wallach R (2020) Effects of time-dependent contact angle on wettability of subcritically water-repellent soils. Water Resour Res 56:e2020WR027314. https://doi.org/10.1029/2020WR027314

Wang J, Ghimire R, Fu X, Sainju UM, Liu W (2018) Straw mulching increases precipitation storage rather than water use efficiency and dryland winter wheat yield. Agric Water Manage 206:95–101. https://doi.org/10.1016/j.agwat.2018.05.004

Wang D, Li C, Parikh SJ, Scow KM (2019) Impact of biochar on water retention of two agricultural soils - a multi-scale analysis. Geoderma 340:185–191. https://doi.org/10.1016/j.geoderma.2019.01.012

Wang H, Wang F, Li ZC, Zheng Y, Gu TR, Zhang RN, Jiang ZY (2023) In situ reaction enabled surface segregation toward dual-heterogeneous antifouling membranes for oil-water separation. J Hazard Mater 460:132425. https://doi.org/10.1016/j.jhazmat.2023.132425

Watson C, Schlösser C, Vögerl J, Wichern F (2021) Hydrochar, digestate, and process water impacts on a soil's microbial community, processes, and metal bioavailability. Soil Sci Soc Am J 85:717–731. https://doi.org/10.1002/saj2.20239

Wu YQ, Yang S (2023) Experimental basis for determining contact angle in the ideal model of unsaturated soils. Soil till Res 227:105602. https://doi.org/10.1016/j.still.2022.105602

Wu TT, Mo LJ, Yan YB, Hu YX, Liu KZ, Chen D (2025) Study on the evaporation characteristics of self-rewetting droplets on different wettability surfaces. Int J Therm Sci 211:109698. https://doi.org/10.1016/j.ijthermalsci.2025.109698

Xu H, Shan YD, Ling N, Ren LX, Qu HY, Liu ZP, Xu GH (2023) Divergent effects of food waste derived hydrochar on hydraulic properties and infiltration in a sandy soil. J Hydrol 626:130267. https://doi.org/10.1016/j.jhydrol.2023.130267

Xu MP, Liu YY, Xi JZ, Li SQ, Li ZY (2024) Optimization of soil hydrological properties in degraded grasslands by soil amendments. J Hydrol 643:131946. https://doi.org/10.1016/j.jhydrol.2024.131946

Xue Y, Gao B, Yao Y, Inyang M, Zhang M, Zimmerman AR, Ro KS (2012) Hydrogen peroxide modification enhances the ability of biochar (hydrochar) produced from hydrothermal carbonization of peanut hull to remove aqueous heavy metals: batch and column tests. Chem Eng J 200–202:673–680. https://doi.org/10.1016/j.cej.2012.06.116

Yang CD, Lu SG (2021) Effects of five different biochars on aggregation, water retention and mechanical properties of paddy soil: a field experiment of three-season crops. Soil till Res 205:104798. https://doi.org/10.1016/j.still.2020.104798

Zhang X, Shi F, Niu J, Jiang YG, Wang ZQ (2008) Superhydrophobic surfaces: from structural control to functional application. J Mater Chem 18:621–633. https://doi.org/10.1039/b711226b

Zhang K, Mao JF, Chen BL (2019) Reconsideration of heterostructures of biochars: morphology, particle size, elemental composition, reactivity and toxicity. Environ Pollut 254:113017. https://doi.org/10.1016/j.envpol.2019.113017

Zhang KZ, Zhang K, Li YM, Kang QL, Wang YF, Wang J, Yang K, Mao JF (2023) Easily pyrolyzable biomass components significantly affect the physicochemical properties and water-holding capacity of the pyrolyzed biochar. Agriculture 13:2053. https://doi.org/10.3390/agriculture13112053

Zhang DX, Jie HB, Zhang WJ, Yuan QS, Ma ZH, Wu HZ, Rao W, Liu SL, Wang DC (2024) Combined biochar and water-retaining agent application increased soil water retention capacity and maize seedling drought resistance in Fluvisols. Sci Total Environ 907:167885. https://doi.org/10.1016/j.scitotenv.2023.167885

Zhang PZ, Chang FL, Huo LL, Yao ZL, Luo J (2025) Impacts of biochar pyrolysis temperature, particle size, and application rate on water retention of loess in the semiarid region. Water 17:69. https://doi.org/10.3390/w17010069